ISIJ International, Vol. 36 (1996), No. 1, pp. 7–16

# Prediction of the Optimum Bubble Size for Inclusion Removal from Molten Steel by Flotation

**Laihua WANG, Hae-Geon LEE and Peter HAYES**

Department of Mining and Metallurgical Engineering, The University of Queensland, St. Lucia, Qld 4072, Australia.
E-mail: laihua@minmet.uq.oz.au

(*Received on May 2, 1995; accepted in final form on July 24, 1995*)

A mathematical model has been developed to determine the optimum bubble size for the removal of inclusions from molten metals by flotation. The probability of collision between a bubble and an inclusion, $P_C$, and the probability of adhesion of an inclusion to a bubble by sliding, $P_A$, are defined to describe the efficiency of inclusion attachment to a bubble. The results show that small bubbles have a high $P_C$, while small inclusions have a high $P_A$ and low $P_C$. By considering the overall probability, $P\,(=P_C \times P_A)$, and the floating time of the bubble, the model suggests that the optimum bubble sizes for the removal from steel of alumina inclusions less than 50 $\mu$m in size are in the range of 0.5 to 2 mm in diameter.

KEY WORDS: bubble/particle interaction; clean steel production; impurity removal; inclusion removal; mathematical modelling; metal refining; optimum bubble size.

## 1. Introduction

Gas injection is commonly practiced in the ferrous and non-ferrous secondary metallurgy processes. This technique is used to achieve homogeneity in the temperature and metal composition and to assist in the removal of second phase and dissolved impurities from molten metals.

Cold modelling[1] has demonstrated that when the particles do not wet the liquid phase, the particles can be captured by gas bubbles and floated up to the free surface. Solid inclusions such as alumina and silica are non-wetted by liquid steel,[2] and can therefore be removed by attachment to gas bubbles.

In general the metallurgical industry has moved towards generating smaller size bubbles in order to improve the efficiency of impurity removal. For example, tuyere and lance injection has been replaced by the use of porous refractory plugs to create smaller gas bubbles. A currently commercialised technology for ultra clean steel production, NK-PERM (NK-Pressure Elevating and Reducing Method),[3] uses alternate pressurisation to create fine bubbles in order to remove inclusions from liquid steel.

It has been assumed that the smaller the bubble size, the higher the efficiency of removal. Intuitively it can be argued that smaller bubbles have a high probability of collision with inclusions, however their lower rising velocity leads to longer floating times. Larger bubbles have a lower probability of collision with inclusions, but having higher rising velocity.

This work is aimed at determining the optimum bubble size for the inclusion removal on the basis of the interaction of gas bubbles with particle inclusions, particularly for the removal of fine, non-wetting inclusions of diameter 5 to 50 $\mu$m.

## 2. Mechanism of Bubble/Inclusion Interaction

The process of inclusion removal by gas bubbles is influenced by various factors including the liquid flow, the properties of inclusion, bubble, molten metal and slag. The overall process is complicated by the coalescence and breaking of bubbles in the bubble swarm. Detailed quantitative modelling of the overall process is not possible at present, but the study of the behaviour of a single bubble in the quiescent liquid steel is a very useful starting point in analysing this problem.

Previous theoretical and experimental studies[4–7] have shown that the overall process of particle flotation by a gas bubble can be divided into several sub-processes:

1) Approach of a particle to a bubble,
2) Formation of a thin liquid film between the particle and the bubble,
3) Oscillation and/or sliding of the particle on the bubble surface,
4) Drainage and rupture of the film with the formation of a dynamic three-phase contact (TPC),
5) Stabilisation of bubble/particle aggregates against external stresses, and
6) Flotation of the bubble/particle aggregates.

Of the above mentioned sub-processes, the attachment of particles to bubbles plays a central role.

For ease of description the following times are defined. The oscillation time of the particle following the initial collision with the bubble surface is the collision time, $t_C$. The time elapsed when the inclusion is sliding over the



© 1996 ISIJ

bubble surface is the sliding time, $t_S$. The time for the drainage of the liquid film between the gas and the inclusion until film rupture occurs is defined as film drainage time, $t_F$.

The processes of attachment of an inclusion to a gas bubble in the liquid steel can also be further understood as follows:

The inclusion approaches the gas bubble, and a thin liquid steel film builds up between the inclusion and the bubble. The film gradually drains until film rupture occurs. If the collision time is longer than the film drainage time, *i.e.*, $t_C > t_F$, the inclusion will be attached by the collision. If $t_C < t_F$, the inclusion will rebound away from the bubble or slide on the bubble surface. If the sliding time is longer than the film drainage time, *i.e.*, $t_S > t_F$, the attachment will occur during sliding. If $t_S < t_F$, on the other hand, the inclusion will slide away and will not become attached to the bubble. In this paper the attachment by collision will be referred to as mechanism (A) and that by sliding as mechanism (B) respectively. These mechanisms are illustrated schematically in **Fig. 1**. Polar coordinates are used to describe location in the following models and the nomenclature used is given at the end of the paper.

## 3. Important Parameters

Preliminary calculations indicate that the models are very sensitive to certain model parameters, such as the terminal velocity of the gas bubble, the collision time, and the film drainage time. Special consideration has therefore been given to these parameters before they are incorporated into the models.

### 3.1. Terminal Velocity of Bubbles

The terminal velocities of gas bubbles in liquid steel, particularly for fine bubbles, are difficult to measure accurately. However, many studies on the terminal velocity of gas bubbles in water have been carried out.

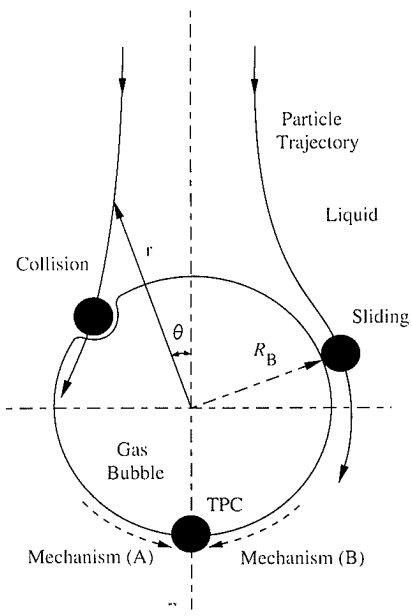


**Fig. 1.** Schematic representation of mechanisms of particle attachment to a gas bubble.

Based on experimental measurements a number of mathematical models of the phenomenon have been developed.[8-10] These models describe the influences of the density, viscosity, surface tension of the liquid, the bubble size and the fluid flow characteristics. Unfortunately, the agreement between these models varies considerably. In the present study an average value of bubble velocity in steel predicted using these models is adopted and then smoothed by the mathematical method of cubic spline fitting. The properties of alumina inclusions, water and steel used in the following calculations are listed in **Table 1**.

**Figure 2** shows the terminal velocities of gas bubble in liquid steel predicted by the different models and the average result. The terminal velocities and shapes of bubbles depend on the bubble sizes. In the regime of bubbles with diameters less than 3 mm, the bubbles are spherical in shape. When the equivalent diameter of the bubble exceeds 3 mm, the bubble becomes ellipsoidal in shape. The bubble velocity reaches a maximum value in the transition region from sphere to ellipsoid. The emphasis in the present work is on the bubble size in the range less than 5 mm in diameter, so that all the bubbles are assumed to be spherical in shape in the following calculations.

### 3.2. Collision Time $t_C$ and Film Drainage Time $t_F$

Schulze[6] derived an expression of collision time, $t_C$, by taking into account non-linear oscillation of particle on the gas bubble surface,

**Table 1.** Physical properties of alumina inclusions, water and steel.

| Properties | Values | Refs. |
|---|---|---|
| $\rho_{H_2O}$ | 1 000 kg/m$^3$ | 15) |
| $\rho_{Fe}$ | 7 000 kg/m$^3$ | 16) |
| $\rho_{Al_2O_3}$ | 3 000 kg/m$^3$ | 16) |
| $\mu_{H_2O}$ | $10^{-3}$ kg/m·s | 15) |
| $\mu_{Fe}$ | $7.0 \times 10^{-3}$ kg/m·s | 16) |
| $\sigma_{H_2O}$ | $7.3 \times 10^{-2}$ N/m | 15) |
| $\sigma_{Fe}$ | 1.89 N/m | 2) |

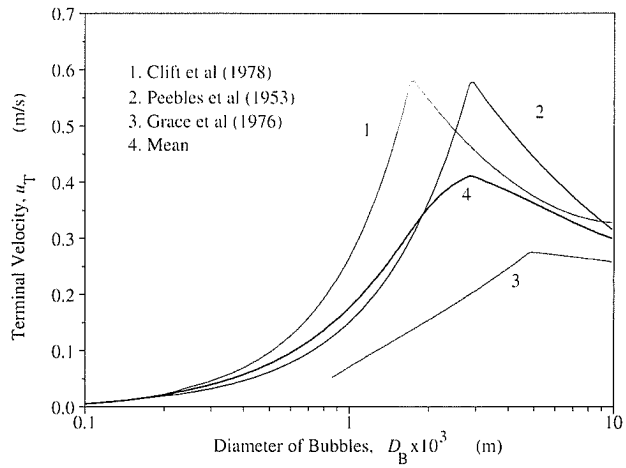


**Fig. 2.** Terminal velocities of gas bubbles in liquid steel as a function of bubble size.

© 1996 ISIJ

$$t_C = \pi f \left[ \frac{(\rho_P + 1.5\rho_L) D_P^3}{24\sigma_L} \right]^{1/2} \quad \text{.....(1)}$$

where $\rho_L$ and $\rho_P$ are the relative densities of the liquid and the particle. The non-linear function $f$ depends on the particle size $D_P$ and the surface tension $\sigma_L$. Inserting the surface tension of liquid steel (Table 1) into Schulze's model,[6] the magnitude of $f$ for steel is 3.6 to 4.2 when the inclusion sizes are in the range of 5 to 50 $\mu$m.

The model for $t_C$ (Eq. (1)) was verified by Schulze's experiments[6] using a pendant water drop and a high-speed camera.

Schulze[6] considered two limiting cases for the calculation of the film drainage time:

1) plane contact: Reynolds' equation in the case of a plane-parallel thin film of finite dimensions, and
2) point contact: Taylor's equation for a solid sphere approaching a rigid wall.

Schulze's model for the evaluations of film drainage time in these two cases can be summarised as:

Plane contact:

$$t_{FR} = \frac{3}{64} \left( \frac{\pi}{180} \right)^2 \frac{b_\alpha^2 (32 u_R t_C)^{2m_\alpha} \mu_L D_P^3}{\sigma_L k h_{Crit}^2} \quad \text{.....(2)}$$

Point contact:

$$t_{FT} = \frac{6\mu_L \ln (D_P / 2h_{Crit})}{\left( 36\mu_L \frac{u_B}{D_B} + \frac{2}{3} D_P \Delta\rho g \right) \cos\theta} \quad \text{.....(3)}$$

$$\Delta\rho = \rho_P - \rho_L \quad \text{.....(4)}$$

where $\mu_L$ and $\sigma_L$ are the viscosity and surface tension of liquid respectively. $\theta$ is the angle in the polar coordinate system as shown in Fig. 1. $u_R$ is the relative velocity of bubble to particle. The factor $k$ takes the value of 4. The constants $b_\alpha$ and $m_\alpha$ depend almost linearly on the particle size, and weakly change with surface tension of the liquid. Therefore $b_\alpha$ and $m_\alpha$ take the values of 700 and 0.6 respectively as recommended by Schulze.[6]

The critical thickness $h_{Crit}$ for the film rupture in Eqs. (2) and (3) can be obtained by an empirical relation based on the experimental results by the interferometrical measurement,[11]

$$h_{Crit} = 2.33 \cdot 10^{-8} [\sigma_L \cdot 10^3 (1 - \cos\theta_A)]^{0.16} \quad \text{.....(5)}$$

where $\theta_A$ is the advancing contact angle, which is substituted with the contact angle in the present calculation, and $\sigma_L$ is liquid surface tension.

**Table 2** lists the results for a typical case of alumina inclusions in steel.

The actual value of $t_F$ should be between the two limiting values, $t_{FR}$ and $t_{FT}$. According to the calculations given in Table 2, $t_C$ is larger than $t_{FR}$ and less than $t_{FT}$. This indicates that $t_C$ may be larger or less than $t_F$, and that the two mechanisms of attachment, (A) and (B) may occur in the process of inclusion attachment to gas bubbles in the steel.

**Table 2.** Calculated contact time and film drainage time for alumina inclusions in steel.

| $D_P$ (m) | $5 \times 10^{-6}$ | $5 \times 10^{-5}$ |
|---|---|---|
| $t_C$ (s) | $3.0 \times 10^{-6}$ | $9.6 \times 10^{-5}$ |
| $t_{FR}$ (s) | $4.7 \times 10^{-10}$ | $2.9 \times 10^{-5}$ |
| $t_{FT}$ (s) | $3.1 \times 10^{-3}$ | $5.3 \times 10^{-3}$ |

Conditions: $D_B = 2$ mm, $\theta = 0^0$, $\theta_C = 144^\circ$ (Ref. 2)).

## 4. Mathematical Model

In the model presented in this paper, the possibilities of rebound of the inclusion from the bubble surface following the first collision and the detachment of the inclusion from the bubble after the formation of three phase contact are neglected. Experimental results obtained by Pan[1] using non-wetting particles in aqueous solutions show that almost all of the particles arriving at the bubble surface become attached. Solid inclusions such as alumina and silica are not wetted by liquid steel (the contact angles of alumina and silica inclusions with liquid steel are 144° and 115° respectively[2]). It is therefore assumed that analogous behaviour occurs in the high temperature process.

The probability that an inclusion will collide with a bubble is defined as collision probability, $P_C$, and the probability of adhesion by sliding is defined as adhesion probability, $P_A$. The overall probability of attachment of the inclusion to the bubble, $P$, is given by the product of these probabilities, *i.e.*,

$$P = P_C \cdot P_A \quad \text{.....(6)}$$

### 4.1. Collision Probability, $P_C$

Whether an inclusion approaches a bubble depends principally on the fluid flow around the bubble. Consider the case of an isolated bubble rising through a suspension of inclusions in a quiescent environment. As the liquid sweeps past the bubble, a flow pattern represented by the infinite series of streamlines as shown in **Fig. 3** develops in the fluid. For mathematical convenience, this can be considered to be analogous to a

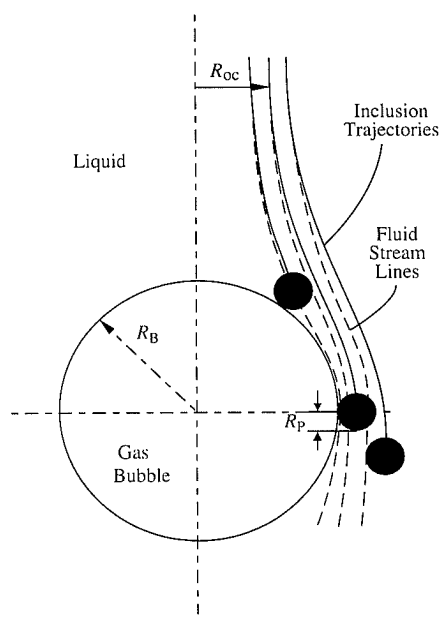


**Fig. 3.** Schematic representation of collision of particles with a bubble.



© 1996 ISIJ

stationary bubble around which the fluid is moving at a velocity equal to the terminal rising velocity of the bubble but in the opposite direction.

The trajectory of an inclusion is considered to be determined by the streamline which passes through its centre. Assuming that the streamlines come closest to the bubble at its equator, a grazing streamline is defined as the one passing through the bubble at the distance of inclusion radius, $R_P$, at the equator. This streamline originated at the distance of $R_{0C}$ from the central axis at an infinite distance from the bubble. It is clear that, of the inclusions located in the path of the bubble, only those within the limiting radius, $R_{0C}$, will collide with the bubble. Those which lie outside this area will sweep past the bubble without having an opportunity for contact. The collision probability is therefore determined by the ratio of the area $A_{0C}(=\pi R_{0C}^2)$ to the area $A_{BP}[=\pi(R_B+R_P)^2]$. Thus, the collision probability is given as:

$$P_C=\frac{A_{0C}}{A_{BP}}=\frac{R_{0C}^2}{(R_B+R_P)^2} \quad (D_P<D_B) \quad \text{.....(7)}$$

The value of $R_{0C}$ is unknown and must be determined from the mathematical description of the grazing streamline.

Studies of fluid flow around a spherical obstruction, *e.g.*, drop and bubble, have been reported in the literature.[4-6] In the cases of low Reynolds numbers (much less than unity) and very high Reynolds numbers, it is possible to obtain analytical solutions to Navier–Stokes equations. For the case of intermediate Reynolds numbers, *i.e.*, $1<\mathrm{Re}<500$, numerical solutions have to be used.

Various simplifications of the velocity profile around the bubble have been made by Yoon,[4] Weber[5] and Schulze[6] in their models. The complexities of the mathematical expressions of the collision probability vary from model to model depending on how the description of the flow pattern is simplified, but the predictions using these models are quite close to each other if applied to the same case. Of these models, that developed by Yoon[4] is relatively simple. It involves the fitting of an empirical equation of stream function to experimental data available in the literature in the range of $1<\mathrm{Re}<100$. But when the inclusion sizes are close to bubble sizes, the probability predicted by this model exceeds unity. In the present work, Yoon's expression for $P_C$ has been modified by including the higher order terms and considering the effect of relative velocity (Appendix 1):

$$P_C=\frac{1}{1-u^*}\left[\frac{3}{2}+D^*+\frac{2\mathrm{Re}^{0.72}(2+D^*)}{15(1+D^*)}\right]\frac{D^{*2}}{(1+D^*)^3} \quad (D_P<D_B) \quad \text{.....(8)}$$

where

$$u^*=\frac{u_P}{u_B} \quad \text{.....(9)}$$

and

$$D^*=\frac{D_P}{D_B} \quad \text{.....(10)}$$

As suggested by Yoon,[4] this expression is also applicable to the case of $\mathrm{Re}>100$.

### 4.2. Adhesion Probability, $P_A$

After collision with the bubble the inclusion begins to slide over the bubble surface and stays on the surface for a finite period of time. The residence time is referred to as sliding time, $t_S$. The magnitude of the sliding time is determined by the tangential component of the relative velocity and the bubble size since larger bubbles have longer sliding distances. A number of measurements of sliding time have been reported.[12]

Bubble/inclusion attachment will occur when the sliding time $t_S$ is longer than the film drainage time $t_F$. Therefore, the inclusion must slide a finite distance over the bubble surface before the attachment occurs. In reference to **Fig. 4**, for given size of bubble and inclusion, the distance travelled by an inclusion along the surface of a bubble is a function of the incidence angle $\theta_I$, at which the inclusion strikes the bubble. Only when $\theta_I$ is smaller than the limiting angle, $\theta_{OA}$, will the inclusion have a sliding time longer than the film drainage time and become attached. The probability of adhesion of the inclusion to the bubble by sliding, $P_A$, will be the ratio of the area inscribed by the limiting radius, $R_{OA}$, to the area inscribed by the sum of the bubble radius with inclusion's, $R_B+R_P$. Thus $P_A$ can be expressed as (Appendix 1):

$$P_A=\frac{R_{OA}^2}{(R_B+R_P)^2}=\sin^2\theta_{OA} \quad (D_P<D_B) \quad \text{.....(11)}$$

By taking the same stream function as Yoon's[4] mentioned in the foregoing section, Yoon's expression of $P_A$ can be modified as:

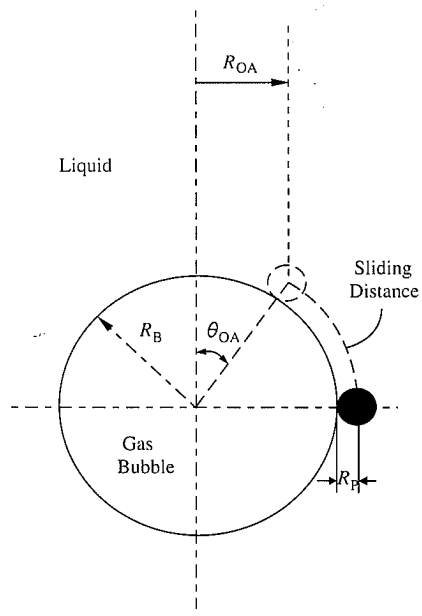


**Fig. 4.** Schematic drawing showing the critical angle of incidence and the probability of adhesion.

© 1996 ISIJ

$$P_A = \sin^2\left[2\arctan\exp\left(-\frac{2t_F}{D_B+D_P}\left\{\left[1-\frac{3}{4x_E}-\frac{1}{4x_E^3}+\frac{Re^{0.72}}{15}\left(-\frac{2}{x_E^4}+\frac{1}{x_E^3}+\frac{1}{x_E}\right)\right](u_B-u_P)\right\}\right)\right] \quad \ldots(12)$$

where

$$x_E = 1 + D^* \quad (D_P < D_B) \quad \ldots\ldots(13)$$

## 5. Results and Discussions

The probability of collision, $P_C$, can be obtained from Eq. (8). **Figure 5** shows the relationship between $P_C$ and bubble size for a range of inclusion diameters from 5 to 50 $\mu$m. $P_C$ increases with decreasing bubble size and with increasing inclusion size, *viz*, smaller bubbles have higher probability of collision with an inclusion of given size than larger bubbles, and larger inclusions have higher probability of collision with a given size bubble than smaller inclusions.

The magnitude of $P_C$ is determined by the fluid flow around the gas bubble. For the movement of a viscous liquid about a bubble, the flow pattern of fluid can be represented by an infinite series of streamlines, as shown in Fig. 3. From geometric considerations it can be seen that the ratio of $R_{OC}/(R_B+R_P)$ for a large bubble is lower than that for a small bubble. So, according to Eq. (7) $P_C$ increases as the size of bubble decreases. $P_C$ for 20 $\mu$m inclusions at bubble diameters 1 mm is only 0.5%. This means that only one bubble in 200 (=1/0.005) bubbles with diameter of 1 mm will collide with an inclusion of 20 $\mu$m in a column of fluid 1 mm diameter, *i.e.*, the same as that swept out by the bubble.

According to Eq. (12), the value of adhesion probability, $P_A$, depends on the magnitude of the film drainage time, $t_F$, while $t_F$ itself is determined by the bubble and particle sizes according to Eqs. (2) and (3). The adhesion probability, $P_A$, can be obtained by solving the Eqs. (12) with (2) or (3). Taking the maximum value of $t_F$ given by Eq. (3), $P_A$ is illustrated as a function of bubble and inclusion size in **Fig. 6** for inclusion sizes in the range of 5 to 50 $\mu$m. The effect of bubble size on $P_A$ varies with inclusion size. For inclusions 5 to 10 $\mu$m in diameter there is no significant influence of the bubble size on $P_A$, *i.e.*, $P_A$ is effectively independent of the bubble size. In the case of larger inclusions, *i.e.*, 20 to 50 $\mu$m in diameter, both the small and large bubbles have a higher $P_A$ than intermediate size bubbles. This is due to the low rising velocity in the case of the small bubbles and the long sliding distance offered by the large bubbles both of which favour the adhesion of the inclusions. From Fig. 2, the bubbles with a diameter around 2 to 3 mm have a high rising velocity, so that the $P_A$ is minimum under this condition.

For inclusions greater than 10 $\mu$m in diameter, $P_A$ significantly decreases with the increase in inclusion size (Fig. 6). This indicates that smaller inclusions are more easily captured by a gas bubble during sliding. $P_A$ of the inclusions with 5 to 10 $\mu$m diameter is high over the whole range of bubble size from 1 to 5 mm diameter. This is the result of the high gradient of velocity close to the bubble surface.[13] In the present calculations, the sliding velocity of an inclusion is taken as the tangential velocity of the fluid around the gas bubble and at a position corresponding to the centre of the inclusion, so that a small inclusion has a lower sliding velocity and hence a longer sliding time. On the other hand, since both the inclusion and the bubble float up in the same direction in the liquid steel and a smaller inclusion has a slower rising velocity than a larger inclusion, the relative velocity of a small inclusion to the rising bubble is larger than that of a large inclusion to the bubble. This results in a reverse influence on the attachment of the smaller inclusion to that mentioned above in relation to the tangential velocity, but it is comparatively less important than the contribution from the tangential velocity.

As mentioned above, the value of $P_A$ depends on the magnitude of $t_F$. High $t_F$ results in a low $P_A$. Low $t_F$ means that the film ruptures easily. Zero $t_F$ means that once an inclusion approaches a bubble, it will be attached immediately, in which case the $P_A$ is equal to one. Two limiting cases for $t_F$ are given by Eqs. (2) and (3). In the results as shown in Fig. 6, $t_F$ has been taken to be the upper limiting value given by Eq. (3), so that the $P_A$ given in Fig. 6 is a low limit. The real $P_A$ should be

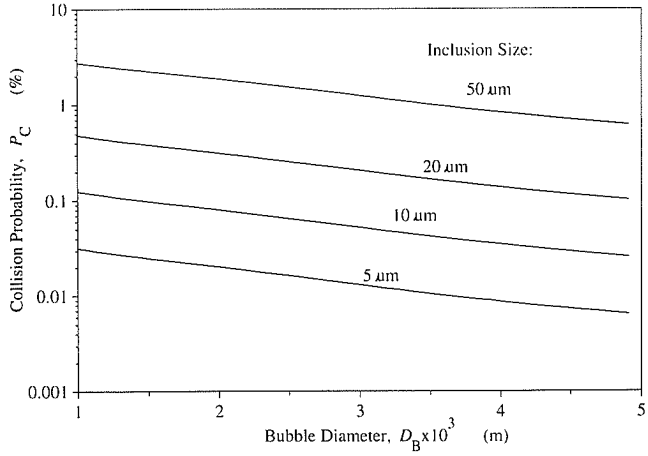


**Fig. 5.** Probability by collision of inclusions with gas bubbles as a function of bubble size and inclusion size.

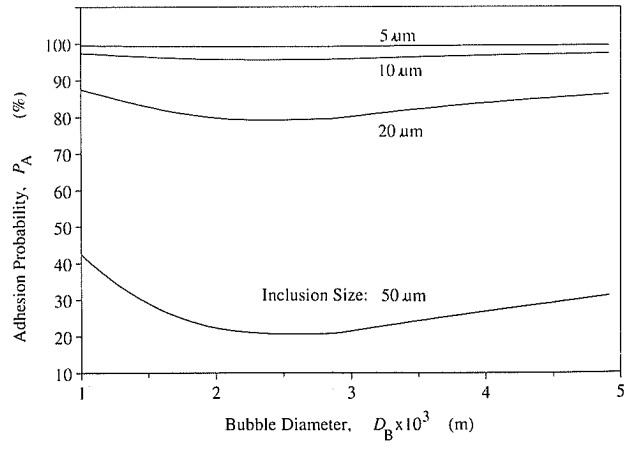


**Fig. 6.** Probability by adhesion of inclusions sliding on the surface of bubbles as a function of bubble size and inclusion size.



© 1996 ISIJ

higher than the values given in Fig. 6.

To understand the stability of the inclusion attachment to a gas bubble, the position of the inclusion on the bubble surface has been further calculated. The position of the inclusion on the bubble surface is expressed as the ratio of the depth of the inclusion wetted by liquid steel to its diameter, *i.e.*, $y/D_B \times 100\%$ as shown in **Fig. 7**. By considering the balance of the forces acting on the inclusion, as listed in the Appendix 2, the position of an inclusion can be calculated as a function of bubble and inclusion size (**Fig. 8**). When the bubble size is larger than 0.5 mm in diameter, less than 20% of the diameter of the inclusion is contained in the liquid steel regardless of inclusion size and bubble size. In the case of small bubbles, *i.e.*, less than 0.4 mm in diameter, both decreasing the bubble size and increasing the inclusion size will obviously increase the proportion of the inclusion in the steel. These influences are due to the effects of the capillary force and interfacial tension. The lower the proportion of inclusion wetted by steel, the more likely the inclusion will not become detached from the bubbles. Therefore the bubbles larger than 0.5 mm favour the retention of the inclusion in the bubble/inclusion aggregates.

The efficiency of the inclusion removal can be furthermore expressed as the injected gas volume required to remove all inclusions. In the imaginary liquid column through which the bubble is passing, if the probability of an inclusion to be attached to the bubble is $P$, the number of bubbles to obtain a unit probability should be $N_B = 1/P$. The number of columns for a unit cross-section of vessels (such as ladle or tundish) is $N_C = 4/(\pi D_B^2)$. The total number of gas bubbles required to remove all inclusions is therefore $N_T = N_B \cdot N_C$. The theoretical gas volume, $V_T$, to remove all the inclusions per unit cross-section of vessels is thus:

$$V_T = N_T \frac{\pi D_B^3}{6} = \frac{2D_B}{3P} \quad \text{.....(14)}$$

where $P$ is obtained from Eq. (6). Equation (14) is also applicable to the case of more than one inclusion with same size in the column.

The theoretical gas volumes, $V_T$, in two cases of inclusion sizes 10 and 50 $\mu$m are illustrated in **Figs. 9** and **10** respectively. The lower lines in these two figures represent the mechanism (A) as mentioned before, *i.e.*, attachment by collision, by which $P_A = 1$, thus $P$ is equal to $P_C$. The upper lines represent the mechanism (B), *i.e.*, adhesion by sliding, by which $P_A < 1$. The real gas volume should be between these two limits.

Figure 9 shows that in the case of a small inclusion of 10 $\mu$m in diameter, curve (B) is very close to curve (A), which is due to the low film drainage time $t_F$ of small inclusions (Table 2). This indicates that the small

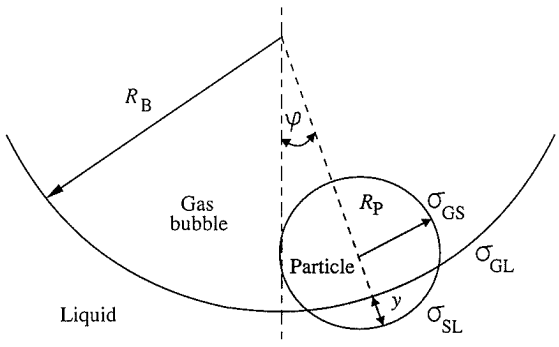


**Fig. 7.** Schematic representation of a particle attached and detached from a gas bubble.

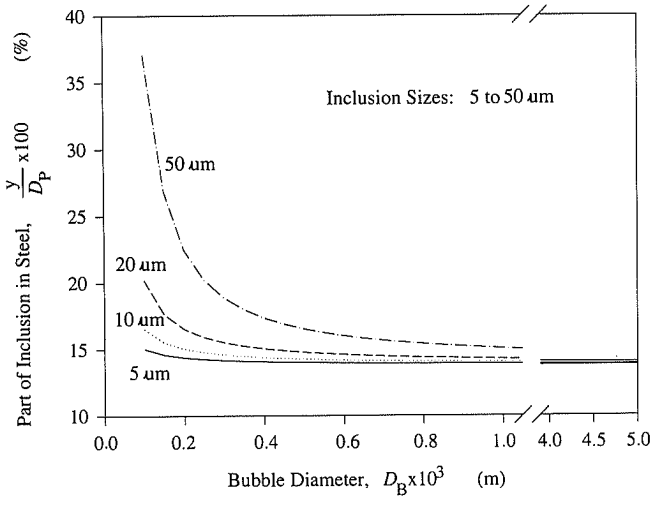


**Fig. 8.** The equilibrium position of an alumina inclusion in liquid steel attached to a gas bubble.

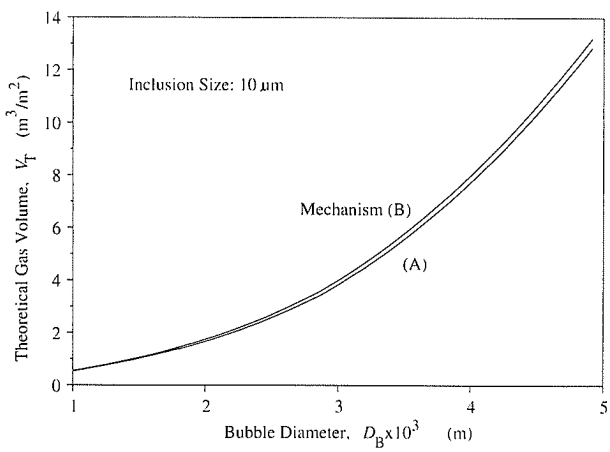


**Fig. 9.** Theoretical gas volume per unit area for the removal of all inclusions as a function of bubble sizes.

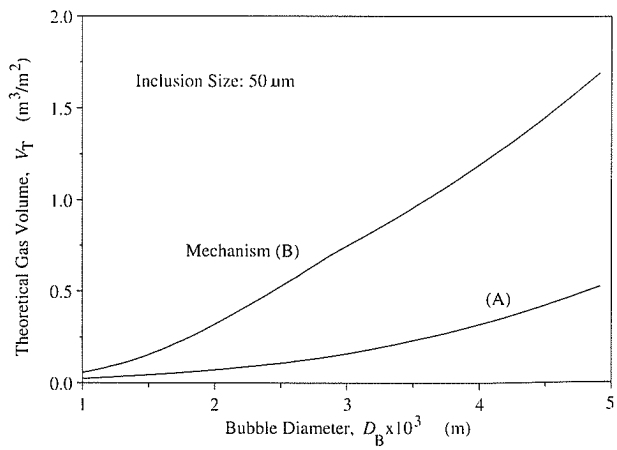


**Fig. 10.** Theoretical gas volume per unit area for the removal of all inclusions as a function of bubble sizes.

© 1996 ISIJ

inclusions are easily attached by the first collision. For inclusions of 50 $\mu$m in diameter, there is a difference of the gas volumes $V_T$ between mechanisms (A) and (B), as shown in Fig. 10. This is due to the higher $t_F$ value for the larger inclusions.

**Figure 11** shows the theoretical gas volume, $V_T$, required by mechanisms (B) for the inclusion of 5 to 50 $\mu$m diameter. As shown in Fig. 11, the gas volume, $V_T$, required for the total removal of fine inclusions, *e.g.* 5 $\mu$m, rapidly increases for bubble sizes larger than 2 mm.

**Figure 12** shows the bubble terminal velocities and their rising times for passing through one meter liquid steel, $t_R$. Small bubbles have a low rising velocities and thus require a long floating time. For gas injection into the ladle, a flow pattern with recirculating zone and stagnant zone is inevitably developed. The small bubbles with a low rising velocity may be trapped in the recirculating zone or stay in the stagnant zone and therefore the inclusions attached to these bubbles do not have any chance of being floated to the covering slag layer. The horizontal velocity of liquid steel near the slag and metal interface is generally 0.1 m/s.[17,18] To avoid being entrained into the bulk, the bubbles need to have a faster vertical velocity than 0.1 m/s. According to Fig. 12, the bubble rising time for bubble size smaller than 0.5 mm rapidly increases with decreasing bubble size. To obtain a vertical velocity higher than 0.1 m/s the gas bubbles should be larger than 0.5 mm in diameter. In practice, shorter treatment time of liquid steel will significantly reduce the operational costs by reducing the temperature loss and refractory consumption. For these reasons, bubbles smaller than 0.5 mm are undesirable.

In the current practice in the industry, nozzles, tuyeres or porous plugs are used to introduce gas into the metallurgical vessels. The average sizes of bubbles are 10 to 20 mm. According to the above calculations, the gas volumes required to remove the same number of inclusions with 10 to 20 mm diameter bubbles will be 150 to 200 times more than these using small bubbles of 0.5 to 2 mm in diameter.

By considering the stability of bubble/particle aggregates as shown in Fig. 8, the rising time of the gas bubbles as drawn in Fig. 12 and the efficiency for the inclusion removal as illustrated in Fig. 11, it may be concluded that the optimum bubble sizes for the efficient removal of inclusions less than 50 $\mu$m are in the range of 0.5 to 2 mm in diameter.

Once the inclusion is attached to the bubbles the probability that it will become detached in a turbulent flow region have also been considered. The detachment actually depends on the relative velocity of the inclusion to the gas bubble. The conditions for detachment can be calculated by considering the force balance on the particle, including surface tension, inertial force, gravity and capillary forces. The details of the model are listed in the appendix. The results are illustrated in **Fig. 13**. The critical relative velocity is defined as the relative velocity between bubble and particle at which an inclusion will be detached from the bubble. As shown in Fig. 13, the critical velocities are almost independent of bubble size and the larger inclusions are the more easily detached from the bubbles. The inclusions of 50 $\mu$m in size will not become detached until the relative velocity is greater than 18 m/s, which is much higher than the velocity of any bulk flow in the ladle or tundish. This indicates that the detachment will not happen under the

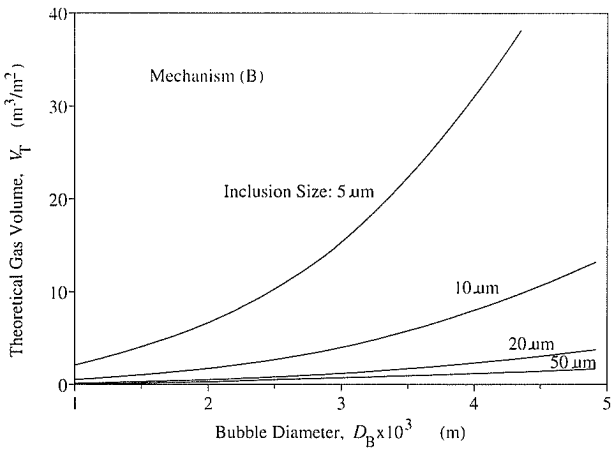


**Fig. 11.** Theoretical gas volume per unit area for the removal of all inclusions as a function of bubble size for mechanism (B).

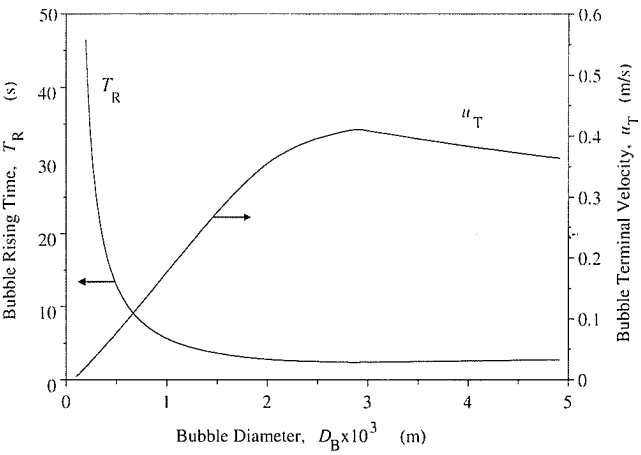


**Fig. 12.** Rising time of bubbles through one meter liquid steel and bubble terminal velocity as a function of bubble size.

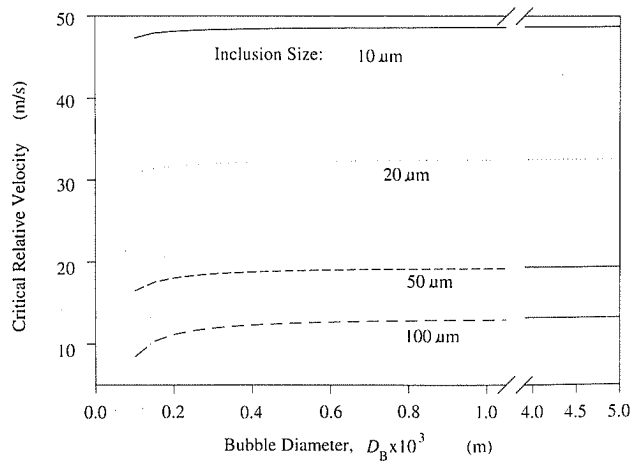


**Fig. 13.** Critical relative velocity for an inclusion to be detached from bubble into steel.



© 1996 ISIJ

existing operational conditions in the steelmaking process.

## 6. Conclusions

A mathematical model has been developed to predict the efficiency of removal of alumina inclusions from steel by considering the bubble/particle interaction. The model predicts that:

(1) The collision probability, $P_C$, increases with decreasing bubble size and increasing inclusion size.

(2) The adhesion probability, $P_A$, is influenced by bubble and inclusion size. In the case of larger inclusion sizes, *i.e.*, 20 to 50 $\mu$m, $P_A$ reaches a local minimum value with the bubbles approximately 2 to 3 mm in diameter. When the inclusion sizes are smaller than 10 $\mu$m, $P_A$ is independent of bubble size. Smaller inclusions have a higher $P_A$ than the larger inclusions.

(3) The theoretical gas volume per unit cross-section of liquid steel to remove all of the inclusions, $V_T$, decreases with decreasing bubble sizes.

(4) The optimum efficiency of flotation of inclusions is obtained using bubble diameters between 0.5 to 2 mm.

**Acknowledgments**

The authors gratefully acknowledge the financial support provided by the Department of Employment, Education and Training (DEET), Commonwealth Government of Australia under the Targeted Institutional Links Program.

The authors would also like to thank members of 1) POSTECH and POSCO of Korea, and 2) BHP Steel, HiSmelt Corp. and CRA of Australia for their advice on the development of this project.

**Nomenclature**

$D$: Diameter (m)
$E$: Total surface energy (N/m)
$F$: Force (N)
$g$: Gravity constant (m/s$^2$)
$h_{Crit}$: Critical thickness of liquid film (m)
$P_A, P_C$: Probabilities of adhesion and collision
$R$: Radius (m)
Re: Reynolds number
$t_C, t_S$: Contact time and slide time (s)
$t_F$: Film drainage time (s)
$t_R$: Bubble rising time passing through one meter liquid steel (s)
$u$: Velocity (m/s)
$u_R$: Relative velocity of bubble to particle (m/s)
$u_T$: Terminal velocity of bubble (m/s)
$u_t$: Tangential velocity of the streamline (m/s)
$V_T$: Gas volume per unit cross-section of molten metal to remove all of the inclusions (m$^3$/m$^2$)
$\rho$: Density (kg/m$^3$)
$\sigma$: Surface tension or interfacial tension (N/m)
$\mu$: Viscosity (kg/m·s)
$\theta, \varphi$: Angle (rad)
$\theta_C, \theta_i$: Contact angle and incidence angle (rad)
$\Psi$: Stream function (m$^3$/s)

Subscript
$Al_2O_3$: Alumina
B: Bubble
Fe: Steel
G: Gas
$H_2O$: Water
L: Liquid
P: Particle
S: Solid

## REFERENCES

1) W. Pan, K.-I. Uemura and S. Koyama: *Tetsu-to-Hagané*, **78** (1992), No. 8, 87.
2) A. W. Cramb and I. Jimbo: *I&SM*, (1989), June, 43.
3) H. Matsuno, Y. Kikuchi, M. Komatsu, M. Arai, K. Watanabe and H. Nakashima: 1993 Steelmaking Conf. Proc., Iron and Steel Society, Inc., PA 15086, U.S.A., **76** (1993), 123.
4) R. H. Yoon and G. H. Luttrell: *Mineral Process. and Extractive Metall. Rev.*, **5** (1989), 101.
5) M. E. Weber and D. Paddock: *J. Colloid Interface Science*, **94** (1983), No. 2, 328.
6) H. J. Schulze: *Mineral Process. Extractive Metall. Rev.*, **5** (1989), 43.
7) H. J. Schulze: *Adv. Colloid Interface Sci.*, **40** (1992), 283.
8) R. Clift, J. R. Grace and M. E. Weber: Bubbles, Drops and Particles, Academic Press, New York, (1978), Eqs. (5-28) and (7-3).
9) J. R. Grace, T. Wairegi and T. H. Nguyen: *Trans. Inst. Chem. Eng.*, **54** (1976), 167.
10) F. N. Peebles and H. J. Garber: *Chem. Eng. Prog.*, **49** (1953), 88.
11) H. J. Schulze and J. O. Birzer: *Colloids Surf.*, **24** (1987), 209.
12) H. J. Schulze: Physicochemical Elementary Processes in Flotation, Elsevier, Amsterdam, (1978).
13) L. E. Seeley, R. L. Hummel and J. W. Smith: *J. Fluid Mech.*, **68** (1975), No. 3, 591.
14) T. A. Engh, H. Sandberg, A. Hultkvist and L. G. Norberg: *Scand. J. Metall.*, **1** (1972), 103.
15) CRC Handbook of Chemistry and Physics, 64th Ed., CRC Press, Inc., Boca Raton, Florida, (1983–1984).
16) Y. Kawai and Y. Shiraishi: Handbook of Physico-Chemical Properties at High Temperatures, ISIJ, Tokyo, (1988), 11, 24 and 105.
17) S. Joo: Ph. D. Thesis, McGill University, Montreal, Canada, (1989).
18) T.-C., Hsiao, T. Lehner and B. Kjellberg: *Scand. J. Metall.*, **8** (1980), 105.

## Appendix 1. Derivations for the Expressions of $P_C$ and $P_A$

By combining the Stokes and potential flow equations, Yoon[4] developed an empirical stream function for intermediate Reynolds numbers ($\Psi$) as follows:

$$\Psi = u_B R_B^2 \sin^2\theta \left[ \frac{1}{2}x^2 - \frac{3}{4}x + \frac{1}{4x} + \frac{\mathrm{Re}^{0.72}}{15}\left( \frac{1}{x^2} - \frac{1}{x} + x - 1 \right) \right] \quad \text{..... (A-1)}$$

where $x = r/R_B$. When $\theta = 90°$, $r = R_P + R_B$, and therefore $x = x_E = 1 + D_P/D_B$ (Fig. 1).

At a distance of far ahead of the bubble,

$$\sin\theta = \frac{R_{OC}}{r} \quad \text{..... (A-2)}$$

which can be substituted into Eq. (A-1) to yield,

$$R_{OC}^2 = \frac{2\Psi}{u_B} \quad \text{..... (A-3)}$$

© 1996 ISIJ

By combining Eqs. (7), (A-1) and (A-3) and considering $u^*$, Eq. (8) can be obtained.

By considering the flotation of the particle, the tangential velocity of the particle at a distance of one particle radius from the bubble surface $u_{tp}$ will be:

$$u_{tp}=u_t-u_P\sin\theta \quad \text{..... (A-4)}$$

where $u_t$ is the tangential velocity of the streamline.

The particle sliding time ($t_S$) can then be expressed as:

$$t_S=\int_{\theta_{OA}}^{\pi/2}\frac{R_B+R_P}{u_{tp}}\,d\theta \quad \text{..... (A-5)}$$

Replacing the equations used in Yoon's model[4] with Eqs. (A-4) and (A-5) and following Yoon's derivation procedures, Eq. (12) can be obtained.

## Appendix 2. Forces Acting on an Inclusion Attached to a Gas Bubble

The attachment and detachment of an inclusion from a gas bubble depends on the balance of the forces acting on it. Considering a spherical inclusion and a spherical bubble as illustrated in Fig. 7, $y$ represents the portion of solid particle in the liquid.

The forces acting on the inclusion particle include:

Inertial force:

$$F_I=\frac{4}{3}\pi R_P^3\rho_P\frac{du_R}{dt} \quad \text{..... (A-6)}$$

where $R_P$ is the radius of the particle, $\rho_P$ is the density of the particle, $t$ is time, and $u_R$ is the velocity of the particle relative to the bubble. When the bubble velocity is zero, $u_R$ is the particle velocity.

Gravitational force:

$$F_W=\frac{4}{3}\pi R_P^3\rho_P g\cos\varphi \quad \text{.....(A-7)}$$

where $\varphi$ is the angle defined in Fig. 7.

Buoyancy force:

$$F_B=-\frac{1}{3}\pi y^2(3R_P-y)\rho_L g\cos\varphi \quad \text{.....(A-8)}$$

The force due to surface tension effects can be obtained by taking the surface area change.

Interfacial Tension:

$$F_{IT}=-\frac{\partial E}{\partial y}=-2\pi R_P\sigma_{GL}\left[-\left(1-\frac{y}{R_P}\right)+\frac{\sigma_{SL}-\sigma_{GS}}{\sigma_{GL}}\right] \quad \text{.....(A-9)}$$

where $E$ is the total surface energy, which is a function of the penetration depth and is expressed as[14]:

$$E=\pi\{-(2R_Py-y^2)\sigma_{GL}+2R_P[y\sigma_{SL}+\sigma_{GS}(2R_P-y)]\} \quad \text{.....(A-10)}$$

The capillary force is the result of the pressure of the gas on the inclusion intruding into the bubble, which gives:

$$F_C=\frac{2\sigma_{GL}}{R_B}\pi y(2R_P-y) \quad \text{.....(A-11)}$$

Drag force:

$$F_D=-C_D\pi R_P^2\frac{1}{2}\rho_L u_R^2 \quad \text{.....(A-12)}$$

where $C_D$ is the drag coefficient, which is given by Clift *et al.*[8] (page 112):

A force balance for the particle gives:

$$F_I=F_W+F_B+F_{IT}+F_C+F_D \quad \text{.....(A-13)}$$

Substituting $F_I$, $F_W$, $F_B$, $F_{IT}$, $F_C$, and $F_D$ in Eq. (A-13) with Eqs. (A-6) to (A-12), and using the following conversion,

$$\frac{du_R}{dt}=\frac{du_R}{dy}\frac{dy}{dt}=u_R\frac{du_R}{dy}=\frac{1}{2}\frac{du_R^2}{dy} \quad \text{.....(A-14)}$$

the following equation is obtained:

$$\frac{du_R^2}{dy}-A_1u_R^2=A_2y^3+A_3y^2+A_4y+A_5 \quad \text{.....(A-15)}$$

where $A_1$ to $A_5$ are:

$$A_1=-\frac{3C_D}{4\rho^*R_P} \quad \text{.....(A-16)}$$

$$A_2=\frac{g\cos\varphi}{2\rho^*R_P^3} \quad \text{.....(A-17)}$$

$$A_3=-\frac{3}{R_P^2}\left(\frac{g\cos\varphi}{2\rho^*}+\frac{\sigma_{GL}}{\rho_PR_BR_P}\right) \quad \text{.....(A-18)}$$

$$A_4=\frac{3\sigma_{GL}}{\rho_PR_P^2}\left(\frac{2}{R_B}-\frac{1}{R_P}\right) \quad \text{.....(A-19)}$$

$$A_5=2g\cos\varphi-\frac{3\sigma_{GL}}{\rho_PR_P^2}\left(\frac{\sigma_{SL}-\sigma_{GS}}{\sigma_{GL}}-1\right) \quad \text{.....(A-20)}$$

and

$$\rho^*=\frac{\rho_P}{\rho_L} \quad \text{.....(A-21)}$$

Integration of Eq. (A-15) gives

$$u_R^2=-\frac{1}{A_1}\left\{A_2y^3+A_3y^2+A_4y+A_5+\frac{1}{A_1}\left[3A_2y^2+2A_3y+A_4+\frac{1}{A_1}\left(6A_2y+2A_3+\frac{6A_2}{A_1}\right)\right]\right\}+C_1e^{Ay} \quad \text{....(A-22)}$$

where $C_1$ is the integration constant.

1) Detachment of a Particle from the Bubble

In a high turbulent flow region, the particle may be detached from the bubble if the relative velocity between the particle and the bubble exceeds a critical magnitude.

When $y=2r_p$, the particle is considered to be detached from the bubble. Inserting zero value of $u_R$ into Eq. (A-21) when $y=2r_p$, $C_1$ is obtained as:

$$C_1=\frac{1}{A_1}\exp(-2A_1R_P)\left\{8A_2R_P^3+4A_3R_P^2+2A_4R_P+A_5\right.$$



© 1996 ISIJ

$$+\frac{1}{A_1}\left[12A_2R_P^2+4A_3R_P+A_4 +\frac{1}{A_1}\left(12A_2R_P+2A_3+\frac{6A_2}{A_1}\right)\right]\Bigg\} \quad \text{.....(A-23)}$$

Substituting Eq. (A-23) into Eq. (A-22) and solving numerically, the critical velocity for the detachment of a particle from a bubble into the liquid can be obtained when $y=0$.

2) Attachment of a Particle to the Bubble

When the position of a particle on a bubble at a steady state is considered, the inertial force and drag force in Eq. (A-13) are zero, which gives:

$$F_W+F_B+F_{IT}+F_C=0 \quad \text{.....(A-24)}$$

Substituting $F_W$, $F_B$, $F_{IT}$ and $F_C$ into Eq. (A-24) and rearranging it gives:

$$-\frac{1}{3}[4\rho_P R_P^3-y^2(3R_P-y)\rho_L]g\cos\theta-\frac{2\sigma_{GL}}{R_B}y(2R_P-y) +2R_P\sigma_{GL}\left(\frac{y}{R_P}-1+\frac{\sigma_{SL}-\sigma_{GS}}{\sigma_{GL}}\right)=0 \quad \text{.....(A-25)}$$

Solving Eq. (A-25) for $y$, the position of a particle at steady state on the bubble surface can be obtained.

© 1996 ISIJ